Wiley Online Library
Early View publication on www.wileyonlinelibrary.com
(issue and page numbers not yet assigned;
citable using Digital Object Identifier – **DOI**)

Phys. Status Solidi A, 1–8 (2016) / **DOI** 10.1002/pssa.201600486

physica status solidi a
www.pss-a.com
applications and materials science

Influence of dopant segregation on the work function and electrical properties of Ge-doped in comparison to Sn-doped In_2O_3 thin films

Karoline L. Hoyer, Andreas H. Hubmann, and Andreas Klein*

Surface Science Division, Institute of Materials Science, Technische Universität Darmstadt, Jovanka-Bontschits-Str. 2, 64287 Darmstadt, Germany

Received 4 July 2016, revised 26 September 2016, accepted 26 September 2016
Published online 20 October 2016

Keywords doping, electrical properties, germanium, In_2O_3, segregation, work function

* Corresponding author: e-mail aklein@surface.tu-darmstadt.de, Phone: +49 6151 16 20772, Fax: +49 6151 16 20771

Ge-doped In_2O_3 thin films prepared by magnetron sputtering are studied using photoelectron spectroscopy and Hall effect measurements. Carrier conductivities of up to 8.35×10^3 S cm^{-1} and carrier mobilities of up to 57 cm^2 V^{-1}s^{-1} are observed. The surface Ge concentration is enhanced by a factor of 2–3 compared to the concentration in the interior of the films. The surface Ge concentration increases with more oxidizing deposition conditions, in opposite to what has been reported for Sn-doped In_2O_3. Ge-doped In_2O_3 films exhibit higher work functions as compared to Sn-doped films, in particular at oxidizing conditions. This is attributed to the formation of a GeO_2 surface phase. While segregation of Sn reduces the carrier mobility due to grain boundary scattering, Ge segregation does not show such an effect. The differences are attributed to the different oxidation states of the segregated dopants, in agreement with the observed dependence of segregation on oxygen activity.

1 Introduction Transparent conductive oxides (TCO) are important electrode materials for organic electronics and solar cells [1–5]. Sn-doped In_2O_3 (ITO) is one of the most prominent TCO materials. Electrical conductivities of $\sim 10^4$ S cm^{-1} are typically obtained by doping with 10 wt.% SnO_2, leading to electron concentrations up to 10^{21} cm^{-3} and a typical electron mobility of 40 cm^2 V^{-1}s^{-1} [6, 7]. At such high dopant concentration, part of the Sn-donors are compensated by oxygen interstitials [8–13]. Other dopants, which have been studied for In_2O_3 are Zr [14–16], Mo [17, 18], W [19], Ti [20], H_2O [15, 21], and Ge [22–24]. Although considerably higher carrier mobilities have been reported with most of these dopants, the obtained conductivities are still lower than those of optimized ITO.

Understanding the limit of electrical conductivity of TCOs would benefit from a better understanding of the role of dopants on the electrical properties of polycrystalline thin films. Apart from an introduction of free carriers, the influence of the dopant species and its concentration on the carrier mobility is only partially resolved. A recent study has suggested that segregation of Sn to grain boundaries noticeably reduces the carrier mobility of ITO [16]. In this context, it is remarkable that Sn dopants have been found both experimentally and theoretically to be mobile already at temperatures as low as 300 °C [25–27]. No information about diffusivity and segregation of other dopants is available. As the ionic radius of Ge^{4+} is smaller than of Sn^{4+} [28], one might expect that Ge is already mobile at lower temperatures than Sn.

Apart from optical transparency, which is guaranteed in In_2O_3 thin films by the band gap of ~2.7 eV and the fact that optical transitions across the fundamental gap are dipole forbidden [29, 30], and electrical properties, the work function ϕ of highly doped In_2O_3 films has been investigated intensively (see Refs. [4, 5, 25, 31–41] and references therein). The work function is particularly important for hole injection into organic conductors, which is a key interface in organic light emitting devices [42].

The work function of a material ϕ has basically two contributions, one from the inner electrostatic potential and one from the surface dipole. The former depends on the Fermi level position with respect to the band edges $E_F - E_{VB}$ and the latter on the atomic details of the surface termination.

The surface termination itself depends on the orientation of the surface.

In order to discriminate between bulk and surface contribution to the changes of work function, both $\phi = E_{vac} - E_F$ and $E_F - E_{VB}$ have to be determined simultaneously. This can be done by photoelectron spectroscopy [40]. How the values are extracted from ultraviolet photoelectron spectra is illustrated in Fig. 5. While the work function is affected by changes in Fermi level and surface dipole, the ionization potential $I_P = E_{vac} - E_{VB} = (E_F - E_{VB}) + \phi$ is affected only by the surface dipole. As adsorbates can influence the surface dipole and surface band bending considerably, a measurement directly after surface preparation without breaking vacuum is mandatory to identify the fundamental parameters influencing the surface potentials [4].

In polar materials like oxides, different principle surface terminations depending on surface polarity can be identified [43, 44]: non-polar surfaces (Tasker type I), polar surfaces with non-polar units perpendicular to the surface (Tasker type II), and true polar surfaces (Tasker type III). The latter are fundamentally unstable in a bulk-terminated configuration and must undergo a reconstruction in order to compensate for the diverging electrostatic potential (polar catastrophe). The In_2O_3 (110) surface corresponds to a type I, the (111) surface to a type II, and the (100) surface to a type III configuration, respectively [45].

The ionization potential of In_2O_3 has been found to significantly depend on surface orientation [4, 45, 46] in agreement with the expected Tasker classification. In addition to this, the surface dipole and hence the ionization potential and work function are expected to be influenced by surface segregation. Together with the significant dependence of ionization potential on surface orientation [4, 45, 46], it is remarkable that the ionization potential of ITO is widely independent on sample preparation and therefore not affected by Sn segregation [25, 40].

In this contribution the surface properties of Ge-doped In_2O_3 (IGO) thin films are systematically studied using photoelectron spectroscopy with *in situ* sample preparation by magnetron sputtering. The results will be compared to studies of Sn-doped In_2O_3 reported previously. The study reveals a significant segregation of Ge to the surface, which is considerably stronger than that reported for Sn-doped In_2O_3 thin films. Moreover, the tendency of an increased surface Sn-concentration upon reduction is opposite for Ge-doped films. IGO films exhibit higher ionization potentials and higher work functions than ITO films, which is attributed to the formation of a GeO_2 surface phase. However, segregation of Ge does not have a remarkable effect on the carrier mobility. This is explained by a more likely segregation of Ge^{4+} to grain boundaries, which do not cause trap states for electrons.

2 Experimental

Thin film deposition and photoelectron spectroscopy were performed in the DArmstadt Integrated SYstem for MATerial research (DAISY-MAT) [4]. The setup combines several deposition chambers with a Physical Electronics PHI 5700 multi-technique surface analysis system with an ultrahigh vacuum sample transfer.

Ge-doped In_2O_3 films were deposited by radio frequency (RF) magnetron sputtering from ceramic 2 in In_2O_3 targets doped with 2, 4, and 6 wt.% GeO_2 (EVOCHEM, purity 99.99%.). The r.f. excitation power was set 25 W and a total pressure of 0.5 Pa was established by adjusting a variable position gate valve with a gas flow of 6.6 sccm. Samples were grown on quartz substrates which were heated via a halogen lamp. The target to substrate distance was 10 cm and deposition times were adjusted to result in film thicknesses of ~200 nm.

X-ray photoelectron spectroscopy (XPS) was carried out using monochromatic Al K_α radiation with an excitation energy of 1486.6 eV. UV photoelectron spectra were recorded in normal emission using He I emission with an excitation energy of 21.22 eV and with a substrate bias of −4 V. In order to avoid sample charging during XPS and UPS measurements, which partially occurs if the deposited film does not have a sufficient electrical contact to the sample holder, Pt contacts were deposited onto the edges of the substrates prior to IGO deposition.

3 Results and discussion

3.1 Surface composition XP survey and core level spectra of Ge-doped In_2O_3 films are shown in Fig. 1. Due to the *in situ* analysis only emissions from In, O, and Ge levels are observed. The spectra are recorded from films deposited at 270 °C with pure Ar as process gas. Such deposition conditions result in highly conductive films with conductivities $>5 \times 10^4$ S cm^{-1}. The In 3d core level shows the characteristic asymmetric shape, which is caused by a partial screening of the excited photoelectrons by the free electron gas [25, 47].

The Ge 2p emission exhibits are rather symmetric shape. Depending on deposition conditions (substrate temperature and oxygen flux), its binding energy varies between 1219.1 and 1220.1 eV. The Ge 3d emission exhibits a quite asymmetric peak shape, which may indicate the presence of two oxidation states (Ge^{4+} and Ge^{2+}). However, the screening by the free carriers might also contribute. This screening could be different for Ge 2p and Ge 3d emissions due to the different surface sensitivities and different core hole lifetimes of the Ge 2p and 3d levels. Taking the maximum of the Ge 3d level as representative for its binding energy, the binding energy of the Ge 3d emission varies between 32.6 and 31.6 eV.

The binding energies of both Ge emissions therefore vary by 1 eV. The same variation is also observed for the binding energies of the In 3d and O 1s emissions. All peaks show parallel shifts. The highest binding energies are obtained for deposition under reducing conditions (pure Ar as process gas). Addition of oxygen to the process gas gradually decreases the binding energies. The parallel shift of all core level binding energies, which are measured in XPS with respect to the Fermi level and which are not affected by surface dipole changes [4, 5, 40], verifies that the shifts are explained by different Fermi level positions rather than by changes of chemical bonding. No significant change of the oxidation

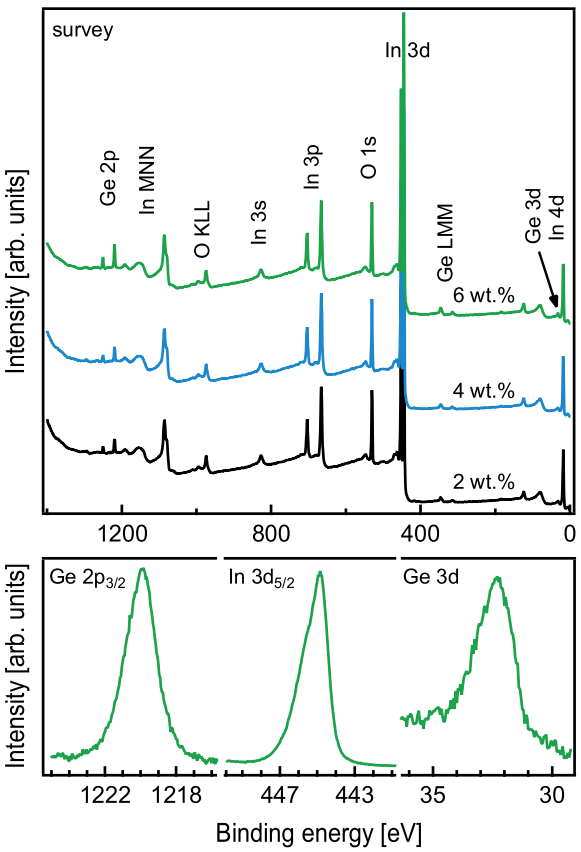

Figure 1 Exemplary XP spectra of Ge-doped In_2O_3 films. All spectra are recorded from samples deposited in pure Ar and at 270 °C substrate temperature. The top graph shows survey spectra from films grown from targets with different amounts of GeO_2 doping. The core level spectra are recorded from the film grown from the target doped with 6 wt.% GeO_2. The zero of binding energy corresponds to the Fermi level position.

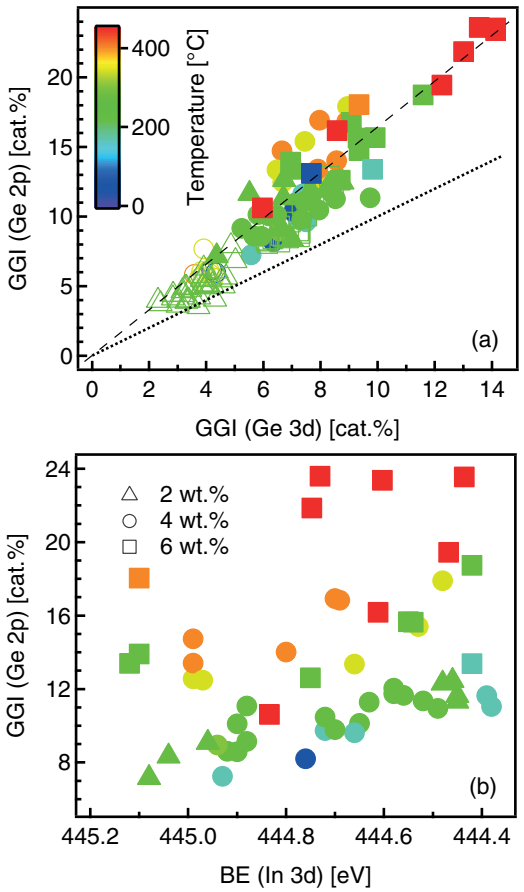

Figure 2 Ge/(Ge + In) (=GGI) ratios of Ge-doped In_2O_3thin films as derived from *in situ* photoelectron spectroscopy. Two different ratios are obtained by taking either the Ge 2p or the Ge 3d core level intensities. The two ratios are compared to each other in (a). The ratio obtained from the Ge 2p level is plotted in (b) against the binding energy of the In 3d level, which is a measure of the Fermi level position of the films. The dashed line (a) is a line going through the origin of the plot. Different symbols and colors correspond to different Ge-contents of the targets and to different substrate temperatures during growth, respectively. Open symbols in (a) correspond to data obtained during *in situ* sputter depth profiling. The dotted line represents the case of equally increasing GGI(Ge 2p) and GGI(Ge 3p).

state of Ge in dependence on deposition conditions is hence indicated.

The compositions of the films were calculated from the peak intensities I, which were normalized with respect to the atomic sensitivity factors A provided by the system manufacturer [48]. The GGI (Ge/(Ge + In)) ratio was obtained using the relation

$$\mathrm{GGI} = \frac{I_{\mathrm{Ge}}/A_{\mathrm{Ge}}}{I_{\mathrm{Ge}}/A_{\mathrm{Ge}} + I_{\mathrm{In}}/A_{\mathrm{In}}}. \quad (1)$$

Due to the strongly different binding energies of the Ge 2p and Ge 3d core levels, the surface sensitivity of the electrons emitted from either level is also strongly different. Using the program NIST Electron Inelastic-Mean-Free-Path Database and the TPP-2M equation [49], the inelastic mean free paths of Ge 2p and Ge 3d photoelectrons amount to 0.76 and 2.50 nm, respectively. The GGI ratios derived using the Ge 2p and the Ge 3d are plotted against each other in Fig. 2a. The data points are arranged along a long line through the origin, which is indicated by the dashed line.

Surface segregation of Ge is first of all evident from that absolute numbers of the GGI as they are much higher than the nominal target compositions, which should correspond to GGI = 2.6, 5.2, and 7.8% for nominal target concentrations of 2, 4, and 6 wt.% GeO_2, respectively. Significantly lower GGI are measured after removal of the surface layer by Ar ion etching (see open symbols in Fig. 2a and the sputter depth profiles presented below). A second strong indicator for Ge surface segregation is the fact that the more surface sensitive Ge 2p peak results in higher GGI than the less surface sensitive Ge 3d. The difference increases with increasing substrate temperature. This is reasonable as higher temperatures should promote dopant segregation by higher mobility of the segregating species.

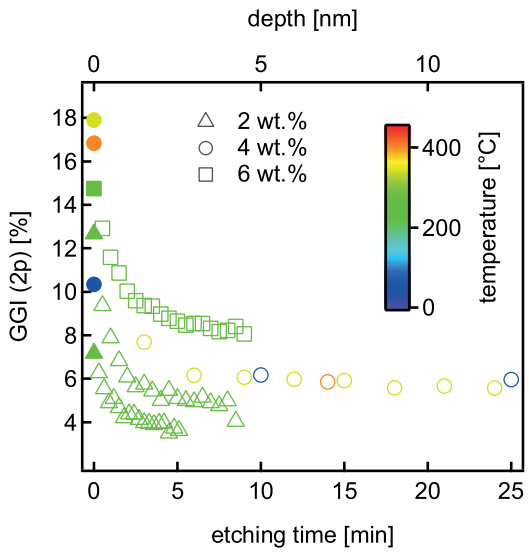

Figure 3 Ge/(Ge + In) (=GGI) ratio of different Ge-doped In_2O_3 thin films as derived from photoelectron spectroscopy with *in situ* sputter depth profiling by Ar ion etching. The etching rate is ~0.5 nm min^{-1}. The top axis shows depth from the surface.

Sputter depth profiling has been performed on a number of samples immediately after deposition by Ar ion etching in the XPS chamber. The results are displayed in Fig. 3. Regardless of initial Ge concentration all samples exhibit a significant decrease of the GGI ratio. The GGI ratio saturates after an etching time of ~5 min. The values are still slightly higher than those expected for the nominal composition of the targets. The latter are better matched by the GGI ratios determined using the Ge 3d intensities. This might also be related to inappropriate atomic sensitivity factors. Nevertheless, the sputter depth profiles clearly support the considerable segregation of Ge on the surface of the growing films.

The surface composition is plotted versus the binding energy of the In 3d core level in Fig. 2b. A high binding energy indicates a high Fermi level position and a high carrier concentration and is obtained with reducing preparation conditions [4, 25, 38]. Correspondingly, a low binding energy indicates a low Fermi level position and low carrier concentration. For given substrate temperature, indicated by the different colors in Fig. 2b, the GGI is clearly increasing with decreasing binding energy. This trend is opposite to what has been observed for Sn-doped In_2O_3, where the surface Sn concentration increases with carrier concentration [16, 25]. Hence, Ge segregation is more pronounced at oxidizing conditions, while Sn segregation is more pronounced at reducing conditions. Another difference between Ge and Sn segregation in IGO and ITO is the fact that no Sn segregation is observed for oxidizing preparation conditions [16, 25], while Ge segregation occurs independent on preparation conditions.

The segregation of Sn upon reduction can be explained by the reduced solubility of Sn. This is caused by the thermodynamic limit for the Fermi level position in doped In_2O_3, which is determined by formation of compensating oxygen interstitials [4, 11–13]. Removing some of the interstitials in highly conductive samples should raise the Fermi level above the level where the formation energy of oxygen interstitials becomes negative. If not enough oxygen is available to compensate for this, the material may alternatively stabilize by excorporating dopants from the crystallographic grains toward the surface or grain boundaries.

The reverse segregation behavior of Ge must have a different origin. It is proposed here that this is related to the higher diffusivity of Ge as compared to Sn in conjunction with oxygen implantation in the growing film. Oxygen ion bombardment of the growing film generally occurs during magnetron sputter deposition of oxides due to negatively ionized oxygen species, which are accelerated toward the substrate by the cathode discharge potential [50]. The bombardment of an In_2O_3 surface with oxygen species leads to the implantation of oxygen, which is likely incorporated as interstitial atoms [12]. This can, for example, be inferred from the observation of surface electron depletion layer [51]. As the ion energy is only a few hundred eV, the implantation is restricted to a sub-surface region. A heavy ion bombardment can result in a very high concentration of oxygen interstitials in the sub-surface region. The oxygen-rich surface layer is not necessarily overgrown by continuing film deposition but may float on the surface if the implanted oxygen is sufficiently mobile. For ITO films this is definitely possible for deposition temperatures above ~200 °C [25–27, 41].

If the Ge atoms are also mobile enough, they can diffuse to the surface and compensate for the charge of the excess oxygen interstitials. The result will then be a GeO_2 layer floating on the surface of the growing IGO film. It has been reported that Sn in ITO is already mobile at 300 °C [25–27, 41]. A higher mobility of Ge as compared to Sn is reasonable due to its smaller ionic radius [28]. Measurements of $GeSb_2Te_4$ phase change material have revealed diffusion of Ge even at room temperature [52].

3.2 Electrical film properties Segregation of Sn also affects the electrical properties of ITO. Apparently, Sn segregates not only to the surface but also to grain boundaries. This is evident from Hall effect measurements at elevated temperatures. Non-monotonic changes of carrier concentrations and mobilities with time are observed in these measurements [26], which cannot be explained if only changes in oxygen content are considered. In addition, highly Sn-doped samples show a reduced carrier mobility and an enhanced grain boundary barrier heights compared to undoped In_2O_3. As Sn segregation occurs preferably under reducing conditions, it is likely that segregated Sn is present as Sn^{2+} and not as Sn^{4+}. A Sn^{2+} on a In^{3+} constitutes an acceptor, which might be the reason for the increase of grain boundary barrier height.

In this work, Hall effect measurements were carried out in van der Pauw geometry only at room temperature. The results of the measurements are compared in Fig. 4 to previously reported data on differently doped In_2O_3 thin films [16]. In general, the data obtained from Ge-doped In_2O_3 are

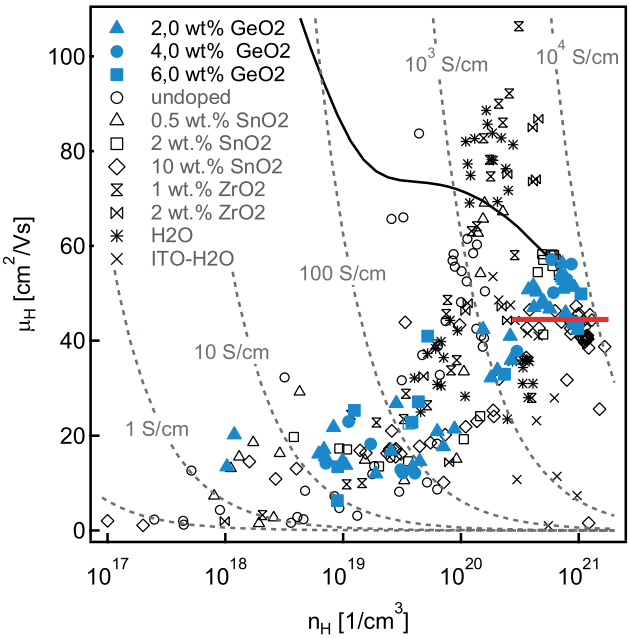

Figure 4 Carrier mobility versus carrier concentration obtained from room temperature Hall effect measurements of Ge-doped In_2O_3 thin films. The measurements are compared to differently doped In_2O_3 films obtained using the same setup [16]. The black solid line corresponds to a calculated dependence of carrier mobility on carrier concentration for single crystalline In_2O_3 using fundamental scattering mechanisms [56]. The red line indicates the dependence of carrier mobility for 10 wt.% SnO_2 doped In_2O_3 films at high carrier concentration.

very much in line with those obtained for films doped with other dopants. The carrier mobility is comparable to those measured for single crystalline films for carrier concentrations $>5 \times 10^{20}\,cm^{-3}$. At such carrier concentrations, the grain boundary barriers are effectively screened by the free electron gas. For lower carrier concentrations, the mobility decreases with decreasing carrier concentration, which is a clear indication for grain boundary scattering [3, 16, 53–55].

The red line in Fig. 4 indicates the dependence of carrier mobility for 10 wt.% SnO_2 doped In_2O_3 films at high carrier concentration. For these carrier concentrations ($3–8 \times 10^{20}\,cm^{-3}$), the mobility of IGO is higher than those of ITO. The highest mobility measured in this work for IGO amounts to $57\,cm^2\,V^{-1}s^{-1}$, which is higher than values obtained by other groups [22–24]. We like to note that potential surface accumulation layers will not contribute significantly to the total conductivity at such high carrier concentrations and a film thickness of 200 nm. The higher mobility therefore indicates a lower influence of grain boundary scattering, in particular a lower concentration of charged traps. As high carrier concentrations in n-doped oxides are obtained under reducing conditions, the higher carrier mobility of IGO compared to ITO is consistent with segregation of Sn^{2+} to grain boundaries in ITO. As Ge segregation increases with more oxidizing conditions, a Ge^{4+} oxidation state of segregated Ge is more likely than a Ge^{2+} oxidation state. Ge^{4+} is a donor when replacing In^{3+} and should therefore not introduce electron traps, which could increase barrier heights at grain boundaries.

The maximum electrical conductivity of IGO achieved in this work is $\sigma = 8.35 \times 10^3\,S\,cm^{-1}$ ($\rho = 1.2 \times 10^{-4}\,\Omega\,cm$), which is close to that obtained for ITO in our previous studies ($\sigma = 1.03 \times 10^4\,S\,cm^{-1}$, $\rho = 9.7 \times 10^{-5}\,\Omega\,cm$) and higher than the conductivity reported in literature [22–24]. The lower conductivity compared to ITO is caused by the higher carrier concentration of ITO. This might be explained by a higher solubility of Sn in In_2O_3 than Ge. This would be in line with the more pronounced Ge segregation at IGO surfaces (up to a factor of 3, see preceding section) as compared to the Sn segregation at ITO surfaces (less than a factor of 2 [16]). However, the highest carrier concentrations of ITO films have been obtained with 10 wt.% SnO_2 doping, which corresponds to a Sn cation concentration of 9.2 %, while the highest doping level used in this study was 6 wt.% GeO_2, which corresponds to a Ge cation concentration of 7.8 %. The fact that both Ge and Sn segregate for dopant concentrations lower than those used for obtaining the highest carrier concentrations also indicate that solubility is not the driving factor for segregation but rather a mechanism like the one proposed in Section 3.1. There may therefore be a potential for higher carrier concentrations in IGO, which may then result in conductivities superior to those of ITO.

3.3 Work function and ionization potential It has to be expected that the significant segregation of Ge or Sn to the surface of IGO or ITO films affects the surface dipole, which should result in a change of ionization potential and work function. These quantities can be extracted from UV photoelectron spectra as indicated in Fig. 5. More details on the extraction of the corresponding values can be found in [4, 5, 40]. Exemplary spectra for different Ge-doped In_2O_3 films are shown in Fig. 5. The work function is extracted from these spectra by subtracting the binding energy of the secondary electron cutoff from the excitation energy of 21.22 eV. The ionization potential is then obtained by adding the binding energy of the valence band maximum to the work function.

The work functions ϕ and ionization potentials I_P of the IGO films are displayed in Fig. 6b and c. For comparison, data from ITO films are shown in Fig. 6a. The dashed line in the plots of ϕ versus E_F indicate a constant ionization potential of 7.7 eV. This line represents well the data for ITO thin films [5, 25, 38]. An ionization potential of 7.7 eV has been identified for the (100) surface orientation of undoped In_2O_3 [45]. ITO films deposited at room temperature also exhibit a clear trend of an ionization potential, which increases with a increasing (100) orientation of the films [4]. However, ITO films grown at 270 °C mostly exhibit a preferential (111) orientation. A lower ionization potential of ~7 eV is expected for this orientation. The IGO films presented in this work also exhibit a preferred (111) orientation with only little

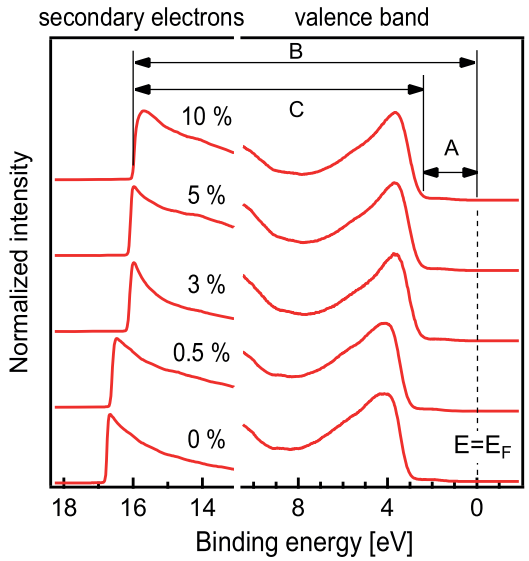

Figure 5 Ultraviolet photoelectron spectra of the secondary electron cutoff (left) and the valence band region (right) recorded *in situ* using He I excitation of IGO films deposited at 270 °C with different amounts of O_2 in the process gas as indicated in %. The binding energies are measured with respect to the Fermi energy E_F. The distance A corresponds directly to the binding energy of the valence band maximum, which is $E_F - E_{VB}$. The work function ϕ is determined from the secondary electron cutoff. The distance B, which is the same as binding energy of the secondary electron cutoff, corresponds to $h\nu - \phi$, where $h\nu = 21.22$ eV is the excitation energy. The ionization potential I_P is finally obtained by $A + \phi = h\nu - C$.

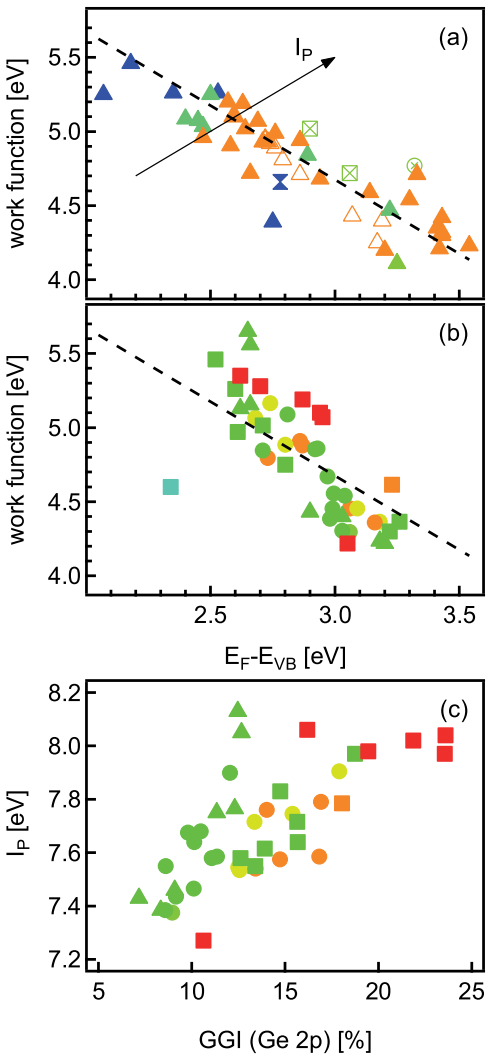

Figure 6 Work function versus Fermi level position of Sn-doped (a) and Ge-doped (b) In_2O_3 thin films measured by *in situ* by photoelectron spectroscopy. The dashed line corresponds to a constant ionization potential of 7.7 eV and the arrow in (a) indicates the direction of increasing ionization potential I_P. The ionization potential is plotted versus the Ge surface concentration in (c). Different colors correspond to different substrate temperatures during film deposition. The color scale is the same as in the other figures.

dependence on deposition conditions. This is in good agreement with literature [22–24]. The ionization potential of ITO and IGO films of ~7.7 eV is higher than the one observed the corresponding In_2O_3 surface [45]. The difference might be caused by an influence of the Fermi level position on surface termination, which is higher for the doped samples [57].

The data for IGO films exhibit a similar trend but with a steeper slope, which indicates that the ionization potential of IGO films increases with decreasing Fermi level position. As the crystallographic orientation of the IGO films is mostly independent on deposition conditions (see X-ray diffraction patterns in the Supplementary Information), it can hardly account for the variation of ionization potential. It is therefore suggested that the higher ionization potential at low Fermi levels is related to a higher Ge surface concentration, which causes an increase of surface dipole. A correlation between Ge surface concentration and ionization potential is indeed suggested by Fig. 6c. The considerably enhanced GGI at the surface of IGO films is very likely related to the appearance of GeO_2 surface phase. The surface dipole will, therefore, no more be determined by the atomic arrangement of In_2O_3, but rather by that of GeO_2.

We are not aware of any measurements of the ionization potential of GeO_2, but the resulting I_P of ~8 eV at low E_F (high GGI) is at the lower limit of the range observed for SnO_2 [58, 59], which has the same oxidation states as GeO_2 and which might form if Sn segregates at ITO surfaces. As indicated by Fig. 6, the ionization potential of IGO can be higher than that of ITO, which offers the potential of obtaining higher work function with IGO, as compared to ITO. This is in line with the study of Kang et al. [24], who observed a similar difference in work function between IGO and ITO.

According to the presented results, this higher work function of IGO is related to the Ge surface segregation. No higher ionization potentials are observed at ITO despite the observed Sn segregation. This can be related to the different trends for segregation. Tin segregates to ITO surfaces under reducing conditions. It is therefore more likely present as Sn^{2+} than as Sn^{4+}. As is well known for SnO_2, the ionization potential of

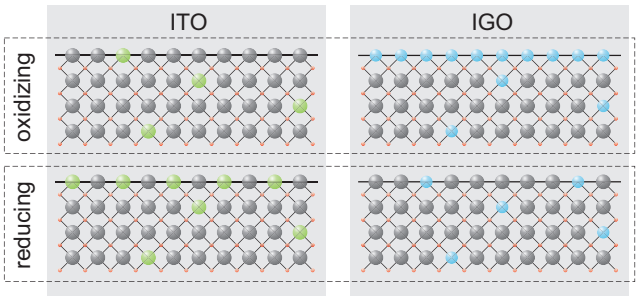

Figure 7 Schematic comparison of dopant distribution in Sn-doped (ITO) and Ge-doped (IGO) In_2O_3 resulting from magnetron sputter deposition under oxidizing and reducing conditions.

reduced SnO_2 surfaces (Sn^{2+}) is considerably lower than that of stoichiometric surfaces (Sn^{4+}) (see [58, 59] and references therein). It is reasonable to assume that segregation of Sn^{2+} in the case of ITO does not have the potential for increasing the surface dipole as has the segregation of Ge^{4+} in the case of IGO.

4 Summary and conclusions Surface and electrical properties of Ge-doped In_2O_3 thin films were studied using photoelectron spectroscopy and Hall effect measurements. In_2O_3 targets with three different Ge concentrations between 2 and 6 wt.% GeO_2 have been used and film properties were further varied by depositing at different substrate temperatures and different O_2 content in the process gas. The surface composition was obtained by quantitative analysis of XPS data and revealed a surface Ge concentration (Ge/(Ge + In)), which is 2–3 times higher than the Ge concentration in the bulk of the films. The latter is confirmed by sputter depth profiling with *in situ* XPS analysis. In contrast to ITO, where the Sn surface concentration increases with more reducing deposition conditions, the surface Ge concentration of IGO films clearly increases with more oxidizing deposition conditions. The amount of surface enhancement is also more pronounced for IGO as compared to ITO. The resulting situation is schematically represented in Fig. 7.

The electrical properties of IGO thin films are comparable to those of ITO. The electrical conductivities of IGO films achieved in this work ($\sigma < 8.35 \times 10^3\,S\,cm^{-1}$) are close to those obtained for ITO in previous studies ($\sigma < 1.03 \times 10^4\,S\,cm^{-1}$). The lower conductivity of IGO films is caused by the lower carrier concentration, which might be related to a lower nominal Ge doping concentration or to a lower solubility of Ge. At high carrier concentrations, IGO films exhibit higher carrier mobilities than highly doped ITO films. In comparison to what has been discussed for ITO [16], this can be ascribed to lower grain boundary barriers. In the case of ITO, an increase of grain boundary barrier height has been related to segregation of Sn^{2+}, which form acceptor states. As Ge segregation increases with more oxidizing conditions, a Ge^{4+} oxidation state is more likely than a Ge^{2+} oxidation state. This could explain why grain boundaries in highly doped IGO films are less detrimental than those in corresponding ITO films.

While ITO films exhibit an ionization potential which is rather independent on deposition conditions, the I_P of IGO films increases with more oxidizing deposition conditions. The increase of the ionization potential of IGO films is correlated with an enhanced Ge surface concentration. This suggests that the higher work function achievable with IGO are related to a GeO_2 surface phase, rather than to a different crystallographic structure of the surface.

Supporting Information Additional supporting information may be found in the online version of this article at the publisher's website.

Acknowledgements This work was supported by the German Bundesministerium für Bildung und Forschung (BMBF) within project 13N13704. Assistance of H.F. Wardenga for the Hall effect measurements is gratefully acknowledged.

References

[1] C. G. Granqvist, Sol. Energy Mater. Sol. Cells **91**, 1529–1598 (2007).
[2] D. S. Ginley, H. Hosono, and D. C. Paine (eds.), Handbook of Transparent Conductors (Springer, New York, 2010).
[3] K. Ellmer, Nature Photon. **6**, 809–817 (2012).
[4] A. Klein, J. Am. Ceram. Soc. **96**, 331–345 (2013).
[5] A. Klein, C. Körber, A. Wachau, F. Säuberlich, Y. Gassenbauer, S. P. Harvey, D. E. Proffit, and T. O. Mason, Materials **3**, 4892–4914 (2010).
[6] I. Hamberg and C. G. Granqvist, J. Appl. Phys. **60**, R123–R159 (1986).
[7] R. B. H. Tahar, T. Ban, Y. Ohya, and Y. Takahashi, J. Appl. Phys. **83**, 2631–2645 (1998).
[8] G. Frank and H. Köstlin, Appl. Phys. A **27**, 197–206 (1982).
[9] N. Yamada, I. Yasui, Y. Shigesato, H. Li, Y. Ujihira, and K. Nomura, Jpn. J. Appl. Phys. **38**, 2856–2862 (1999).
[10] G. B. González, T. O. Mason, J. P. Quintana, O. Warschkow, D. E. Ellis, J. H. Hwang, and J. P. Hodges, J. Appl. Phys. **96**, 3912–3920 (2004).
[11] S. Lany and A. Zunger, Phys. Rev. Lett. **98**, 045501 (2007).
[12] P. Ágoston, P. Erhart, A. Klein, and K. Albe, J. Phys.: Condens. Matter **21**, 455801 (2009).
[13] P. Ágoston, C. Körber, A. Klein, M. J. Puska, R. M. Nieminen, and K. Albe, J. Appl. Phys. **108**, 053511 (2010).
[14] T. Koida and M. Kondo, Appl. Phys. Lett. **89**(8), 082104 (2006).
[15] T. Koida, H. Fujiwara, and M. Kondo, Jpn. J. Appl. Phys. **46**, L685–L687 (2007).
[16] M. V. Frischbier, H. F. Wardenga, M. Weidner, O. Bierwagen, J. Jia, Y. Shigesato, and A. Klein, Thin Solid Films **614**, 62–68 (2016).
[17] C. Warmsingh, Y. Yoshida, D. W. Readey, C. W. Teplin, J. D. Perkins, P. A. Parilla, L. M. Gedvilas, B. M. Keyes, and D. S. Ginley, J. Appl. Phys. **95**(7), 3831–3833 (2004).
[18] D. S. Bhachu, D. O. Scanlon, G. Sankar, T. D. Veal, R. G. Egdell, G. Cibin, A. J. Dent, C. E. Knapp, C. J. Carmalt, and I. P. Parkin, Chem. Mater. **27**, 2788–2796 (2015).

[19] P. F. Newhouse, C. H. Park, D. A. Keszler, J. Tate, and P. S. Nyholm, Appl. Phys. Lett. **87**, 112108 (2005).
[20] M. van Hest, M. S. Dabney, J. D. Perkins, D. S. Ginley, and M. P. Taylor, Appl. Phys. Lett. **87**, 032111 (2005).
[21] H. Wardenga, M. V. Frischbier, M. Morales-Masis, and A. Klein, Materials **8**, 561–574 (2015).
[22] T. Maruyama and T. Tago, Appl. Phys. Lett. **64**, 1395–1397 (1994).
[23] M. Mizuno and T. Miyamoto, Jpn. J. Appl. Phys. **39**, 1849–1854 (2000).
[24] S. B. Kang, J. W. Lim, S. Lee, J. J. Kim, and H. K. Kim, J. Phys. D: Appl. Phys. **45**, 325102 (2012).
[25] Y. Gassenbauer, R. Schafranek, A. Klein, S. Zafeiratos, M. Hävecker, A. Knop-Gericke, and R. Schlögl, Phys. Rev. B **73**, 245312 (2006).
[26] M. V. Hohmann, A. Wachau, and A. Klein, Solid State Ionics **262**, 636–639 (2014).
[27] P. Ágoston and K. Albe, Phys. Rev. B **81**, 195205 (2010).
[28] J. E. Huheey, Inorganic Chemistry: Principles of Structure and Reactivity, 3rd ed. (Harper Collins Publishers, New York, 1983).
[29] A. Walsh, J. L. F. D. Silva, S. H. Wei, C. Körber, A. Klein, L. F. J. Piper, A. DeMasi, K. E. Smith, G. Panaccione, P. Torelli, D. J. Payne, A. Bourlange, and R. G. Egdell, Phys. Rev. Lett. **100**, 167402 (2008).
[30] K. Irmscher, M. Naumann, M. Pietsch, Z. Galazka, R. Uecker, T. Schulz, R. Schewski, M. Albrecht, and R. Fornari, Phys. Status Solidi A **211**, 54–58 (2014).
[31] T. Kugler, W. R. Salaneck, H. Rost, and A. B. Holmes, Chem. Phys. Lett. **310**, 391–396 (1999).
[32] M. G. Mason, L. S. Hung, C. W. Tang, S. T. Lee, K. W. Wong, and M. Wang, J. Appl. Phys. **86**, 1688–1692 (1999).
[33] I. G. Hill, D. Milliron, J. Schwartz, and A. Kahn, Appl. Surf. Sci. **166**, 354–362 (2000).
[34] J. S. Kim, B. Lägel, E. Moons, N. Johansson, I. D. Baikie, W. R. Salaneck, R. H. Friend, and F. Cacialli, Synth. Met. **111-112**, 311–314 (2000).
[35] K. Sugiyama, H. Ishii, Y. Ouchi, and K. Seki, J. Appl. Phys. **87**, 295–298 (2000).
[36] D. J. Milliron, I. G. Hill, C. Shen, A. Kahn, and J. Schwartz, J. Appl. Phys. **87**, 572–576 (2000).
[37] C. Donley, D. Dunphy, D. Paine, C. Carter, K. Nebesny, P. Lee, D. Alloway, and N. R. Armstrong, Langmuir **18**, 450–457 (2002).
[38] S. P. Harvey, T. O. Mason, Y. Gassenbauer, R. Schafranek, and A. Klein, J. Phys. D: Appl. Phys. **39**, 3959–3968 (2006).
[39] S. P. Harvey, T. O. Mason, C. Körber, Y. Gassenbauer, and A. Klein, Appl. Phys. Lett. **92**, 252106 (2008).
[40] A. Klein, C. Körber, A. Wachau, F. Säuberlich, Y. Gassenbauer, R. Schafranek, S. P. Harvey, and T. O. Mason, Thin Solid Films **518**, 1197–1203 (2009).
[41] A. Gassmann, S. V. Yampolskii, A. Klein, K. Albe, N. Vilbrandt, O. Pekkola, Y. A. Genenko, M. Rehahn, and H. von Seggern, Mater. Sci. Eng. B **192**, 26–51 (2015).
[42] B. Minaev, G. Baryshnikov, and H. Agren, Phys. Chem. Chem. Phys. **16**, 1719–1758 (2014).
[43] P. W. Tasker, J. Phys. C **12**, 4977 (1979).
[44] J. Goniakowski, F. Finocchi, and C. Noguera, Rep. Prog. Phys. **71**(1), 016501 (2008).
[45] M. V. Hohmann, P. Ágoston, A. Wachau, T. J. M. Bayer, J. Brötz, K. Albe, and A. Klein, J. Phys.: Condens. Matter **23**, 334203 (2011).
[46] A. Walsh and C. R. A. Catlow, J. Mater. Chem. **20**, 10438–10444 (2010).
[47] C. Körber, V. Krishnakumar, A. Klein, G. Panaccione, P. Torelli, A. Walsh, J. L. F. D. Silva, S. H. Wei, R. G. Egdell, and D. J. Payne, Phys. Rev. B **81**, 165207 (2010).
[48] J. F. Moulder, W. F. Stickle, P. E. Sobol, and K. D. Bomben, Handbook of X-ray Photoelectron Spectroscopy (Physical Electronics, Inc., Eden Prairie, 1995).
[49] U.S. National Institute of Standards, http://www.nist.gov/srd/nist71.cfm.
[50] K. Ellmer and T. Welzel, J. Mater. Res. **27**, 765–779 (2012).
[51] Y. Gassenbauer, A. Wachau, and A. Klein, Phys. Chem. Chem. Phys. **11**, 3049–3054 (2009).
[52] A. Klein, H. Dieker, B. Späth, P. Fons, A. Kolobov, C. Steimer, and M. Wuttig, Phys. Rev. Lett. **100**, 016402 (2008).
[53] J. Y. W. Seto, J. Appl. Phys. **46**, 5247–5254 (1975).
[54] K. Ellmer, J. Phys. D: Appl. Phys. **34**, 3097–3108 (2001).
[55] A. Bikowski and K. Ellmer, J. Appl. Phys. **114**, 063709 (2013).
[56] N. Preissler, O. Bierwagen, A. T. Ramu, and J. S. Speck, Phys. Rev. B **88**, 085305 (2013).
[57] P. Ágoston and K. Albe, Phys. Rev. B **84**, 045311 (2011).
[58] C. Körber, P. Ágoston, and A. Klein, Sens. Actuators B **139**, 665–672 (2009).
[59] K. Rachut, C. Körber, J. Brötz, and A. Klein, Phys. Status Solidi A **211**, 1997–2004 (2014).

